FORSTERITE SHOCK TEMPERATURES AND ENTROPY. E. J. Davies[1], S. Root[2], D. K. Spaulding[1], R. G. Kraus[3], S. T. Stewart[1], S. B. Jacobsen[4], J. P. Townsend[2], P. J. Carter[1]. [1]Department of Earth and Planetary Sciences, U. California, Davis, CA (ejdavies@ucdavis.edu), [2]Sandia National Laboratories, [3]Lawrence Livermore National Laboratory, [4]Department of Earth and Planetary Science, Harvard University

Introduction: Collisions between bodies are important during planet formation [1] and can greatly affect the geochemical evolution of the growing planets [2, 3]. The outcomes of these collisions are dependent on the dynamics of planet formation and the equation of state of the colliding materials. For example, Fig. 1 presents snapshots from a giant impact simulation [4], showing that escaping material is some of the most shocked material during impacts. This escaping material can be tracked in *N*-body simulations.

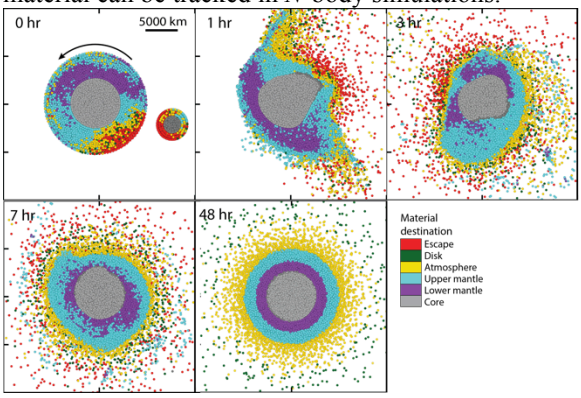

Fig. 1: Giant impact time evolution of an SPH simulation where each particle (dot) represents a fixed amount of mass. Earth-mass body impacted by a 20 km/s half mars-mass projectile. Colors represent the core (gray) and layers in the post-impact state that are tracked through in time. Material in red is the escaping material. Most of the ejecta comes from the impact site and the projectile, making up some of the most highly shocked material in the simulation.

Collisional fragmentation and re-accretion of escaped material was investigated in recent *N*-body simulations of planet formation [5]. In these simulations, the outcomes of collisions and fragmentation between bodies was tracked. During dynamically excited planet formation simulations such as in the Grand Tack model, the majority of collisions disrupt the projectile or erode the target. Even in calmer scenarios, a significant fraction of collisions are still erosive. The total mass of material that is lost during impacts and subsequently re-accreted can be up to half of the mass of the final bodies.

Upon release and expansion into space, the highly shocked ejecta can melt and/or vaporize, potentially leading to the separation of volatile and moderately volatile elements [e.g., 6]. However, there are few constraints on the extent of moderately volatile element depletion in ejecta or the volume of ejecta that is processed. This work attempts to put constraints on the latter. To do this, the fraction of ejecta that is melted and/or vaporized during collisions must be identified for major minerals. We begin with forsterite [Mg_2SiO_4], a major constituent in rocky bodies.

Methods and Results: To predict melting and vaporization of forsterite, the shock Hugoniot must be known. The pressure-volume-temperature (P-V-T) shock state of forsterite was measured on Sandia National Laboratory's Z-Machine as well as the Omega Laser at the University of Rochester [7]. Fig. 2 shows the results of these experiments. There is excellent agreement between the two experimental platforms and density functional theory based molecular dynamics (DFT-MD) calculations. Using these measurements, phase changes can be calculated upon isentropic release to the ambient pressure using the entropy method [8]. However, entropy cannot be measured and must be calculated.

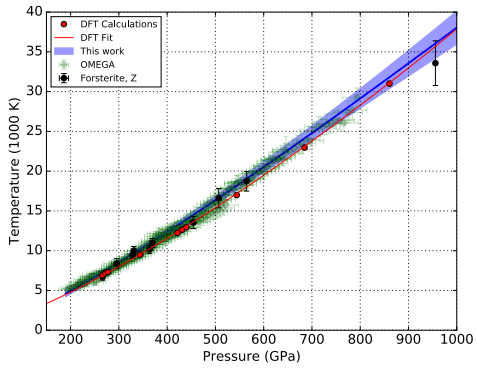

Fig. 2: Shock Hugoniot of forsterite in pressure-temperature space. Red points are DFT-MD calculations, Z-Machine data are in black, and the green colored band is from decaying shock experiments on the Omega laser. The blue line is a fit through the data, with the blue band representing the error envelope. From [7].

To tie the known entropy of forsterite at standard temperature and pressure (STP) to the measured shock Hugoniot, we calculated a thermodynamic integral using published thermodynamic data [9-15]. The following steps of the thermodynamic path are illustrated in Fig. 3. Starting at the entropy at STP (A), forsterite is heated isobarically to the melting point of forsterite at 1 bar (B). The entropy associated with melting is accounted for at (C). From the melting point, the forsterite is heated isochorically to a reference isentrope (D). The isentrope is defined by a third order Birch-Murnaghan equation of state that has been previously used in a number of studies [11-13, 15]. The liquid forsterite is compressed along the isentrope (E) until it

intersects the measured shock Hugoniot at point (F). Once the intersection (F) is known, the entropy along the shock Hugoniot can be calculated by the first law of thermodynamics as shown in Fig. 4.

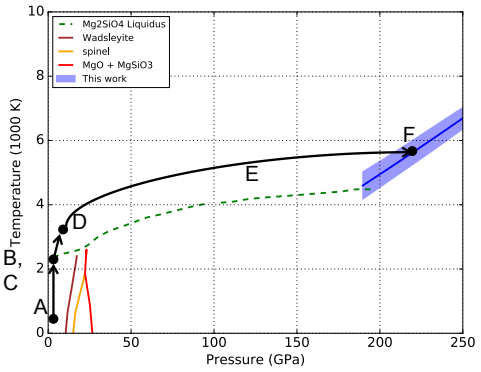

Fig. 3: Simplified phase diagram of the Mg_2SiO_4 system and schematic of the thermodynamic path used for calculating entropy along the Hugoniot. Solid colored lines are the solid-solid phase transitions, the dashed green line is the melt curve. The black line shows the thermodynamic path chosen in this work.

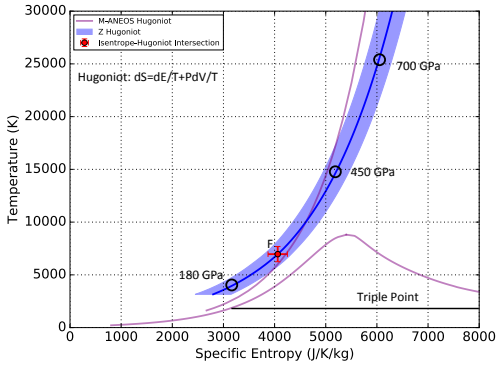

Fig. 4: The measured Hugoniot is shown in blue with its associated error envelope. Purple lines are the predicted Hugoniot and liquid-vapor dome from MANEOS model [16, 17]. Point F is the calculated intersection between the isentrope and Hugoniot. The ambient condition at the triple point is also shown. The MANEOS model is effective at predicting the measured Hugoniot at pressures relevant to planet formation.

Using the entropy method [8], pressures required to reach the onset of melting and vaporization are calculated upon release to 1 bar and the triple point of forsterite, ~5 Pa. Critical impact velocities are derived by assuming rock on rock impacts, using the forsterite shock Hugoniot to find the impact velocities that produce the critical pressures. Table 1 shows the results.

Using the critical impact velocities, we mined the *N*-body simulations from [5] for collisions that exceed the critical velocities for phase changes upon release to the triple point pressure (5.2 Pa, [18]) which is similar to the ambient pressure in the solar nebula. We summed all of the mass ejected during collisions that exceeded the critical impact velocities, shown in Fig. 5. The total system mass that is processed by shock-and-release to vaporization can be up to 50% in dynamically excited systems such as the Grand Tack. The steepness of the orange curve for target bodies between 10^{-4} to 10^{-3} M_{Earth} indicates that most of the processed ejecta comes from energetic collisions between planetesimals.

Amb. P	IM P (GPa)	IM V (km/s)	IV P (GPa)	IV V (km/s)
1 bar	155.27	8.69	230.23	11.13
T.P.	140.31	8.16	178.31	9.49

Table 1: Critical pressures (P) and impact velocities (V) to reach incipient melting (IM) and vaporization (IV).

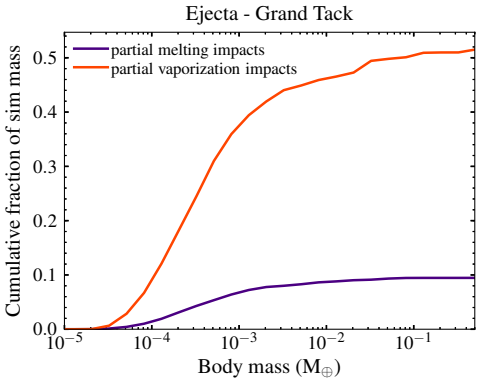

Fig. 5: Cumulative fraction of total simulation mass ejected in collisions that exceed the critical impact velocities against the mass of the target body. In purple are those impacts with velocities that exceed the threshold for the onset of melting, but not of vaporization. In orange, impact velocities that exceed the critical threshold for the onset of vaporization.

Acknowledgments: This work was conducted under the Z Fundamental Science Program. The authors thank the support from DOE-NNSA grant DE-NA0002937 and NASA grants NNX15AH54G and NNX16AP35H. Sandia National Laboratories is a multimission laboratory under contract DE-NA0003525. This work was performed under the auspices of the U.S. Department of Energy by Lawrence Livermore National Laboratory under Contract DE-AC52-07NA27344.

References: [1] Chambers, J. (2010) *Exoplanets* p. 297. [2] Stewart, S.T. and Z.M. Leinhardt (2012) *ApJ* 751, 32. [3] Asphaug, E. (2010) *Chem. Erde* 70, 199. [4] Ćuk, M. and S. T. Stewart. (2012) *Science* 338, 1047. [5] Carter, P. J., et al. (2015) *ApJ* 813, 72. [6] Norris, C. A., and B. J. Wood (2017) *Nature* 549, 507. [7] Root, S., et al. (2017) *JGR* submitted. [8] Ahrens, T. J., and J. D. O'Keefe (1972) *EMP* 4, 214. [9] Robie, R. A., et al. (1982) *AM* 67, 470. [10] Richet, P., et al. (1993) *GRL* 20, 1675. [11] Mosenfelder, J. L., et al. (2009) *JGR* 114, 1203. [12] de Koker, N. P., et al. (2008) *GCA* 72, 1427. [13] De Koker, N. P., et al. (2009) *GJI* 178, 162. [14] Gillet, P., et al. (1991) *JGR* 96, 11805. [15] Thomas, C. W., et al. (2012) *JGR* 117, 10206. [16] Melosh, H. J. (2007) *MAPS* 42, 2079. [17] Canup, R. M. (2012) *Science* 338, 1052. [18] Nagahara, H., et al. (1994) *GCA* 58, 1951.